Pagaimo, MC.; Fernandes, JFP.; Pérez-Sánchez, M.; López Jiménez, PA.; Ramos, HM.; Branco, PJC. (2021). Transient study of series-connected pumps working as turbines in off-grid systems. Energy Conversion and Management. 245:1-15. https://doi.org/10.1016/j.enconman.2021.114586

Transient Study of Series-Connected Pumps Working as Turbines in Off-Grid Systems

Margarida C. Pagaimo[1], João F.P. Fernandes[2*], Modesto Pérez-Sánchez[3], P. Amparo López-Jiménez[3], Helena M. Ramos[4], P. J. Costa Branco[2]

[1] Instituto Superior Técnico, Universidade de Lisboa, Lisboa, 1049-001, Portugal; margarida.pagaimo@tecnico.ulisboa.pt
[2] IDMEC, Instituto Superior Técnico, Universidade de Lisboa, Lisboa, 1049-001, Portugal; joao.f.p.fernandes@tecnico.ulisboa.pt; pbranco@tecnico.ulisboa.pt
[3] Hydraulic and Environmental Engineering Department, Universitat Politècnica de València, Valencia, 46022 Spain; mopesan1@upv.es; palopez@upv.es
[4] Civil Engineering, Architecture and Georesources Department, CERIS, Instituto Superior Técnico, Universidade de Lisboa, Lisboa, 1049-001, Portugal; hramos.ist@gmail.com
[*] Correspondence: joao.f.p.fernandes@tecnico.ulisboa.pt; Tel.: +351 968811445

ABSTRACT

In the current world economic environment where reducing energy costs is a high priority, it is not surprising that sustainable water and energy management are key topics among the water and electric industry. Specifically, water suppliers, pump manufacturers, and operatives of small hydropower systems, all recognize that pumps working as turbines can be an efficient, simple, and economic approach to generating power and recover the excess of energy in water pressurized systems. In both, variable operating flow rate conditions (ex: presence of different water users) impose the need to augment the range of a proper pump as turbine system. One solution is to associate several pumps as turbines in series to increase the recovered energy. In that context, this work assesses their reliability at transient off-grid conditions by two pumps as turbines connected in series. Each one has an identical self-excited induction generator feeding a three-phase and balanced resistive load. Changes (increase/decrease in values) were applied to the resistive loads and the bank of capacitors at one group only, which allowed examining how changes affect the overall two-group system dynamics. Results show that one change in the first pump as turbine group will significantly affect the other group dynamics. For example, a decrease in load of the first group will affect the flow and head of the other system, until reaching a new equilibrium point. However, as both groups are not mechanically connected, they can achieve different equilibrium speeds. Furthermore, the highest impact occurred in the group where no changes were imposed. The first group maintained its global efficiency value, while the second had its efficiency decreased by about 8%. Similarly, an increase in the capacitance value caused a reduction in its efficiency (lesser but around 2%). Finally, a numerical model was developed and validated through experimental tests to be an applicable prediction model.

KEYWORDS: Energy Efficiency; Off-grid PAT; Self-excited Induction Generator (SEIG); Series-connections; water-energy nexus.

1 Introduction

For water distributing systems (WDS)' sustainability studies, the energy implications must be analyzed to improve the efficient use of energy and energy recovery in managing the water systems [1]. The energy consumed in the water cycle is typically distributed on the extraction stage (40 %), the distribution stage (25 %), the wastewater stage (20 %), and the remaining energy are required to supply the consumers [2]. The distribution stage includes the different pipes and elements, which allow consumers to get water according to the pressure and flow necessary to develop their services. The energy of this stage is to compensate for the friction and singular losses of the water

distribution network and the geometric level of the different points on it. In this line, the recycled rates in water networks are expected to be around 22–23% [3]. Optimizing the synergy planning for energy stations and pipeline networks is important to achieve cost savings in WDS [4]. However, when the topography is irregular or the network is large, some points can present high-pressure values, which should be dissipated using pressure reduction valves (PRVs) before supplying consumers [5]. PRVs guarantee users a correct operation range of pressure when they consume the water. However, PRVs are not sustainable since these valves dissipate the excess energy in heat and noise. The use of pumps working as turbines (PATs) was established in recent years as a sustainable alternative solution to PRVs [6]. PATs can recover the excess of hydraulic energy by converting it to electrical [7]. PAT models were developed since 1999, when [8] proposed the use of PATs in the water system to recover energy. This trend led to the development of different simulation models considering the operational curve of the machine [9]. The proposal of empirical expressions to get the best efficiency point of the pump operating as a turbine was proposed to improve the selection method of PATs [10]. These methods were based on computer fluid dynamics analysis and experimental tests, reducing the errors in the prediction of the behavior of the PAT [11]. The knowledge of this empiric coefficient and the development of the operational curves as a function of the flow enables the definition of regulation strategies, increasing the recovered energy in the systems [12].

These researches show that PATs are also a reliable solution in rural and remote areas. The absence of the electrical grid could be compensated with power generation through a PAT system with an electric generator in locations with natural or artificial waterfalls. It can be used in farms or individual houses when the grid supply is difficult or expensive. In these conditions related to isolated and low power, the PATs' feasibility was demonstrated and compared to conventional turbines [13]. Different research studies showed multiple strategies to optimize the location of the PAT system in water networks, considering different optimization functions (e.g., recovered energy and feasibility using PATs at the fixed rotational speed [14], recovering energy under variable rotational speed [15], reduction of leakage [16], pump type selection [17], among others).

In urban systems, Samora et al. estimated a potential recovery between 102 and 262 MWh/year due to the number of systems in Lausanne (Switzerland) [18]. When PAT technology was considered in pressurized irrigation systems, the theoretical recovered energy was 26.51 MWh/year (10 % of the provided energy in the water network) in Vallada (Valencia) [14]. In [19], other irrigation systems were analyzed, identifying 21.05 GWh of potential energy that could have been recovered using micro-hydropower (12.8 % of the consumed energy) for the provinces of Seville and Cordoba, Spain. In Calabria (Italy), one analysis considered the PATs implementation in collective irrigation systems. These recovery systems could provide an important share in electric production, considering 856 MWh/year [20] and chemical plants with an energy recovery equal to 18.95 MWh/year [21]. These works highlight the importance of using the PAT system to increase the energy efficiency of water distribution systems.

From the electric point of view, Williams et al. [22] and Capelo et al. [23] identified the squirrel-cage induction generator as the most appropriate electrical machine to consider for the energy recovery in water distribution systems using PATs. Simplicity, robustness, reliability, and low cost were the main reasons for this choice [24]. For the induction machine to run as a generator, reactive power is required to optimize this reactive source to maximize the active generated power. If connected to the electric grid, the induction generator can draw the magnetizing current (reactive power). However, when operating isolated from the electric grid, capacitors can provide the magnetizing current necessary to supply reactive energy for the rotating magnetic field. This solution is called a self-excited induction generator (SEIG). Hence, when one PAT-SEIG operates isolated from the electric grid, maximization of the global efficiency also must consider both PAT and SEIG behaviors [23]. With this objective, a new step ahead was recently proposed by Fernandes et al. in [25] by developing an optimization procedure to seek the maximum efficiency of the PAT-SEIG when the recovery system operates in isolated conditions. Besides, the analysis of the transient regimes is also important in water pump-storage systems. In [26], a transient model of a multi-unit pumped storage system coupled with the hydraulic system was developed. This research reflected the coupling effect of units during the transient process. Applied to the system's operation, a pump-turbine, a nonlinear dynamic model, was established, providing a new perspective on the modeling of the pump-turbine in the transient processes [27]. [28] established a new nonlinear model to analyze the dynamic response when it operated under random loads, providing theoretical guidance for studying and analyzing the pumped-storage hydropower plant.

Following the previous research done, this work analyses the impact of series connections between different PAT-SEIG systems, considering the modeling of both the hydraulic-mechanic behavior of the PAT and the mechanical-electric behavior of the SEIG. This is an important multidisciplinary research topic due to the need for optimal utilization of PAT-SEIG in WDS. The need for connecting PAT-SEIG in serial appears when there are high values of the recoverable head. One PAT cannot convert the total available head and when several users are present [29]. In this case, it is necessary to connect several PAT groups in serial to reach the maximum available head, maximizing the recovered energy [30]. Therefore, for series-connected PAT groups in off-grid systems, optimization procedures must search the global system efficiency (PAT + electric generator) and not only maximize the hydraulic efficiency. Furthermore, due to its series connections, the change on the electric operating point of one PAT-SEIG system will influence all the other PAT-SEIG systems connected in series. This work aims to characterize these influences on series-connected PAT-SEIG systems, mainly when there are sudden changes of the exciting capacitor and the electric load.

2 Material and Methods

This section presents the materials and methods used to analyze the behavior of PAT-SEIGs connected in series for off-grid electric applications. A set of two identical PATs are used in series, each one connected to an identical Self-Excited Induction Generator (SEIG) and an electric load. With this series connection, sudden changes are applied to the electric load and the exciting capacitor of one PAT-SEIG system. The influence on the overall system dynamic behavior is studied. First, the used SEIG is introduced, showing its main characteristics and its dynamic electromechanical model. The experimental tests performed with the SEIG to validate its electromechanical model are presented. Secondly, the used PAT and its dynamic model are introduced. Experimental tests with the PAT plus its SEIG system are shown to validate the overall PAT-SEIG model system.

2.1 Self-Excited Induction Generator

Fig. 1 demonstrates the off-grid generating system from which one SEIG is inserted (the prime power will be the PAT). The power flow represented in this figure can be interpreted. As the prime mover transfers mechanical power P_{mec} to the shaft, the SEIG's rotor begins to rotate. Then, if the induction machine contains some residual magnetism, the voltage will be induced at the stator terminals. If the capacitors are properly sized, they will provide the induction machine with the reactive power required for voltage to build up Q_s. As excitation is achieved and if the prime mover is delivering enough P_{mec} to the shaft, the SEIG begins to supply the load with active power P_L and, in the case of an inductive load, with reactive power Q_L.

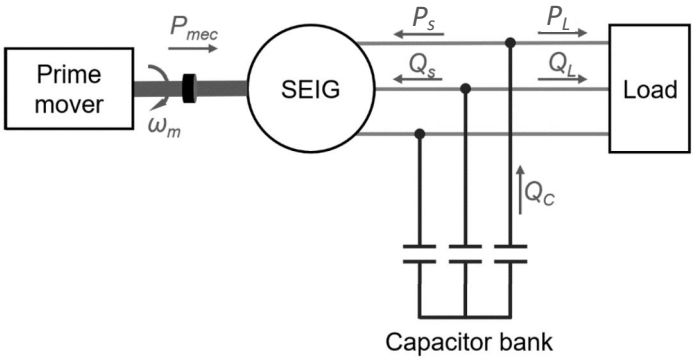

Fig. 1 - Complete isolated power generating system consisting of a prime mover (the PAT system), the self-excited induction generator (SEIG), the capacitor bank, and the electric load.

Fig. 2 shows the star-connected squirrel-cage induction machine used as SEIG, with a rated power of 0.55 kW and rated efficiency of $\eta_N = 68\,\%$. Its nameplate data and equivalent electric parameters are listed in Table 1 and Table 2, respectively. This SEIG was studied in [23]-[25], and the characterization of its equivalent parameters was done. It was noticed that some of these parameters were highly influenced by the magnetization level of the

machine. However, for the PAT-SEIG operation and its power level, the change of the magnetizing inductance, L_m, with the magnetization level, Fig. 3, was the most significant, being enough to characterize the overall system's dynamic behavior accurately.

Fig. 2 – 0.55 kW, 910 rpm, 50 Hz, 2 pair of poles induction machine used for experimental tests.

Table 1 – Nameplate data of the squirrel-cage induction machine.

Frequency	50 Hz
Voltage	400 V
Current	1.6 A
Output Power	0.55 kW
Power factor	0.73
Speed	910 rpm

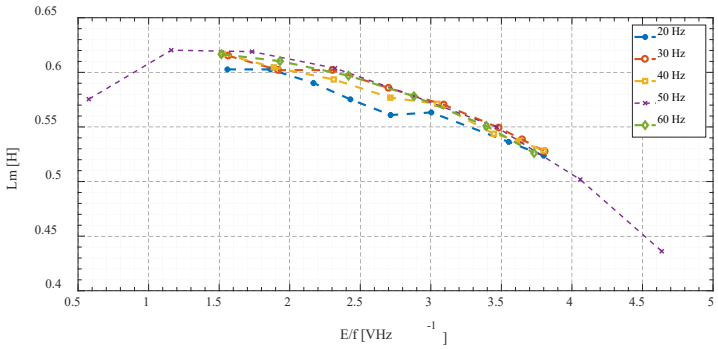

Fig. 3 - Magnetizing inductance, L_m, as a function of the induction machine's magnetization level (E/f). E is the stator voltage, and f is the stator electric frequency.

Table 2 –Induction machine: parameters of its equivalent electric circuit.

Stator resistance, R_s	18.8 Ω
Stator leakage inductance, $l_{\sigma s}$	0.06 H
Rotor resistance, R_s	17.0 Ω
Rotor leakage inductance, $l_{\sigma s}$	0.06 H
Magnetizing resistance, R_m	1700 Ω

A dynamic model of the induction generator is used to understand the transient electromechanical behavior present in the SEIG when coupled to a PAT. Differential equations characterize the induction machine's dynamics with time-varying inductances due to the continuous change with the rotor position with respect to the stator. A new rotating reference frame is considered to decrease the complexity of its dynamic model, accomplished by the direct-quadrature-zero (*dq0*) transformation, Fig. 4. At this point, it will be assumed that the *d*-*q* reference frame is rotating at synchronous angular speed, ω_s. Therefore, when seen from the stator's perspective, the *d*-*q* axis rotates at synchronous angular speed. This implies that the angular displacement of the *d*-axis concerning the stator geometry position will be $\theta = \omega_s t$ at any instant.

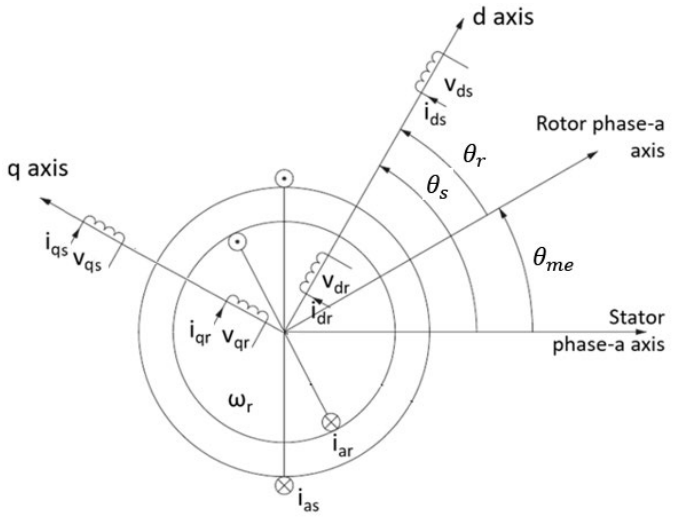

Fig. 4 - Synchronously rotating *d*-*q* reference frame overlapped onto the three-phase reference frame of an induction machine.

Using the synchronous rotating *d-q* reference, the relation between stator and rotor's voltages and currents are given by equations (1)-(4), where u_{ds} and u_{qs} are the stator *d-q* voltages, i_{ds} and i_{qs} are the stator *d-q* currents, i_{dr} and i_{qr} are the rotor *d-q* currents, λ_{ds} and λ_{qs} are the stator *d-q* linkage fluxes, λ_{dr} and λ_{qr} are the rotor *d-q* linkage fluxes, ω_s is the rotating synchronous angular frequency, and ω_r is the electric angular frequency of the rotor related to the *d*-axis. The electrical angular rotor frequency is also given by $\omega_r = \omega_s - \omega_{me}$, with $\omega_{me} = n_{pp}\omega_m$, where $n_{pp}$is the pole pairs and ω_m is the mechanical rotor's angular frequency. R_s and R_r are the stator and rotor electric resistances.

$$u_{ds} = R_s i_{ds} + \frac{d}{dt}\lambda_{ds} - \omega_s \lambda_{qs} \tag{1}$$

$$u_{qs} = R_s i_{qs} + \frac{d}{dt}\lambda_{qs} + \omega_s \lambda_{ds} \tag{2}$$

$$0 = R_s i_{dr} + \frac{d}{dt}\lambda_{dr} - \omega_r \lambda_{qr} \tag{3}$$

$$0 = R_s i_{qr} + \frac{d}{dt}\lambda_{qr} + \omega_r \lambda_{dr} \tag{4}$$

The relations between linkage fluxes and stator currents are given by eq. (5)-(10), where $l_{\sigma s}$ and $l_{\sigma s}$ are the stator and rotor leakage inductances, respectively, and L_m is the magnetizing inductance.

$$\lambda_{ds} = L_s i_{ds} + L_m i_{dr} \tag{5}$$

$$\lambda_{qs} = L_s i_{qs} + L_m i_{qr} \tag{6}$$

$$\lambda_{dr} = L_r i_{dr} + L_m i_{ds} \tag{7}$$

$$\lambda_{qr} = L_r i_{qr} + L_m i_{qs} \tag{8}$$

$$L_s = l_{\sigma s} + L_m \tag{9}$$

$$L_r = l_{\sigma r} + L_m \tag{10}$$

Regarding the magnetizing inductance, L_m, its change with the magnetization level *E/f*, where *E* is the magnetization voltage and *f* the stator electrical frequency, as shown in Fig. 3. For the machine being used in this work (Table 1), its behavior can be approximated by equation (11) for $E/f \in [0\ 4.6]$. Assuming sinusoidal and steady-state quantities, the magnetization level *E/f* is approximately given by $E/f \approx 2\pi\lambda_m/\sqrt{2}$, with the mutual flux λ_m given by $\lambda_m = \sqrt{(\lambda_{ds} - L_s i_{ds})^2 - \left(\lambda_{qs} - L_s i_{qs}\right)^2}$.

$$L_m = 0.0025\left(\frac{E}{f}\right)^3 - 0.041\left(\frac{E}{f}\right)^2 + 0.12\left(\frac{E}{f}\right) + 0.53 \tag{11}$$

The electromagnetic torque developed by the induction machine is determined using (12).

$$T_{em} = \frac{3}{2} n_{pp}\left(\Psi_{ds} i_{qs} - \Psi_{qs} i_{ds}\right) \tag{12}$$

Another important aspect that needs to be modeled is the induced residual stator voltage of the induction machine as a function of its rotor speed. Without this residual stator voltage, the capacitors cannot receive their initial voltage to produce the reactive power required for the induction machine's excitation. This residual stator voltage was measured, following a linear relation with the rotor speed, described by (13), where *N* is the rotor speed in rpm.

$$u_{rem_{rms}} = 0.00086N \tag{13}$$

Finally, as the capacitors are connected in parallel with the induction machine, their voltage, $u_{C_{a,b,c}}$, is the same as the induction machine stator voltage, $u_{s_{a,b,c}}$. Using this, the relation between the SEIG stator current, $i_{s_{a,b,c}}$ and the electric load current, $i_{L_{a,b,c}}$ is defined by (14).

$$u_{s_{a,b,c}} = u_{C_{a,b,c}} = \frac{1}{C}\int i_{C_{a,b,c}} dt + u_{rem_{a,b,c}} = -\frac{1}{C}\int \left(i_{s_{a,b,c}} + i_{L_{a,b,c}}\right) dt + u_{rem_{a,b,c}} \quad (14)$$

2.2 Pump as Turbine

In this research, a radial Etanorm 32-125 KSB 4.8 PAT, Fig. 5(a), is incorporated inside a hydraulic system. The machine is radial, with a specific speed of 51 rpm (m, kW). The best efficiency point of the machine is obtained for the values Q = 3.36 l/s and H = 4 m.w.c. The nominal rotational speed is 1050 rpm, and the impeller diameter was 139 mm, Fig. 5(b). This PAT was used in previous researches [23], [25] and [31], where its characteristic curves, namely the Q-H (flow-head) and the Q-η (flow-efficiency) curves, were experimentally obtained. The PAT interpolated curves are presented in Fig. 6.

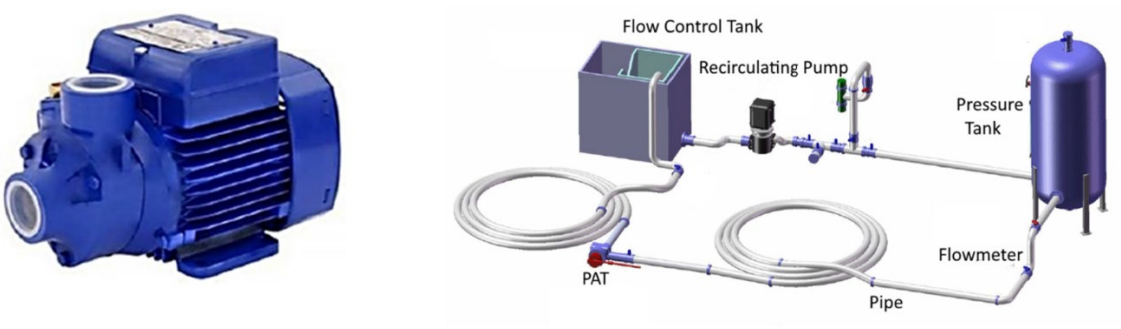

(a) (b)

Fig. 5 – (a) radial Etanorm 32-125 KSB 4.8 PAT, and (b) hydraulic system used to test the PAT.

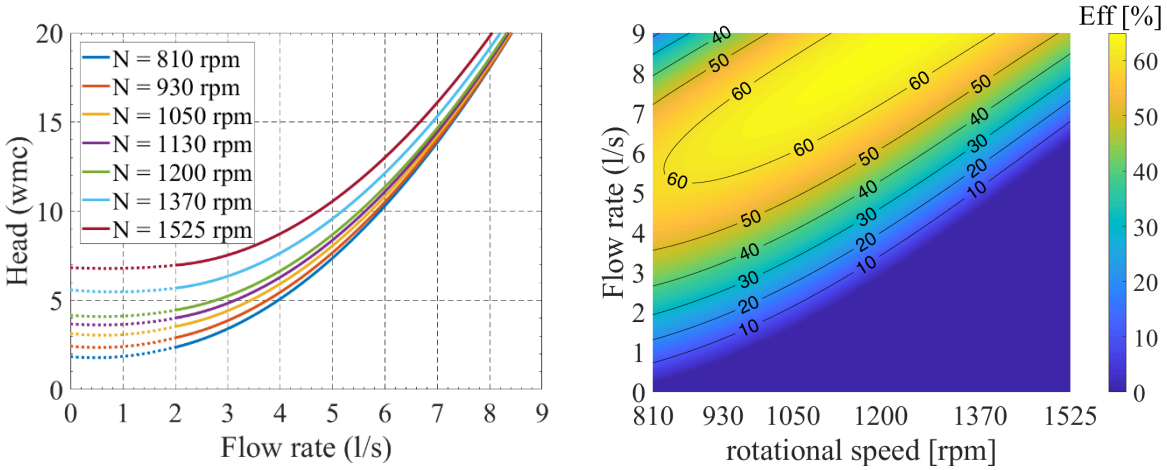

(a) (b)

Fig. 6 – (a) PAT Q-H curves, and (b) PAT Q-η curves.

The typical Q-H curves plotted in Fig. 9(a) can be defined as (15), where α is the ratio between the actual speed, N, and the reference speed, N_{ref}. For this particular PAT, the parameters A, B, and C capable of representing the experimental curves are A = 3.6644, B = -694.45, and C = 314560, for the PAT rated speed of $N_N = N_{ref}$ = 1050 rpm. These results were obtained experimentally for flow rates between 2 to 8 l/s (dashed lines are extrapolations).

$$H = \alpha^2 A + \alpha B Q + C Q^2, \qquad \alpha = \frac{N}{N_{ref}} \quad (15)$$

In the experimental setup utilized in [23], the pressure was the hydraulic parameter that was imposed on the system. For the sake of simplicity, it was admitted that the pressure imposed on the hydraulic system equals the differential fluid pressure between the inlet and outlet of the PAT, P. This relates with the head pressure drop H as $P = \rho g H$. Given this, the characteristic curves had to be adapted to be defined as a head H function instead of the flow rate Q. Therefore, by inverting equation (15), one obtains the H-Q function (16).

$$Q = \frac{-\alpha B \pm \sqrt{(\alpha B)^2 - 4C(\alpha^2 A - H)}}{2C} \tag{16}$$

The function representing the PAT efficiency, $\eta(N, Q)$, was defined by an interpolated surface curve obtained from experimental data plotted in Fig. 9(b). This surface enables the estimation of the efficiency of the PAT even for points that were not experimentally measured.

With the imposed pressure, P, and head, H, and the rotational speed originated from PAT and SEIG coupling, N, the flow, Q, is computed by (16). After, the hydraulic power, P_h, and hydraulic torque, T_h, are determined using (17), where ω_m is the PAT speed in rad/s. With the PAT efficiency and hydraulic torque, the mechanical torque, T_{mec}, is obtained using (18) where η_{PAT} is the PAT efficiency. The connection between the PAT and SEIG is made through mechanical equation (19), where J is the total inertia of the PAT-SEIG system and $T_{losses} = 1.0 \times 10^{-4} \omega_m$.

$$P_h = \rho g Q H, \qquad T_h = \frac{P_h}{\omega_m} \tag{17}$$

$$T_{mec} = T_h \eta_{PAT} \tag{18}$$

$$J \frac{d\omega_m}{dt} = T_{mec} - T_{el} - T_{losses} \tag{19}$$

A schematic of the PAT-SEIG system dynamic model is shown in Fig. 7. After defining the PAT and SEIG models, the system was validated with the experimental results obtained in [23].

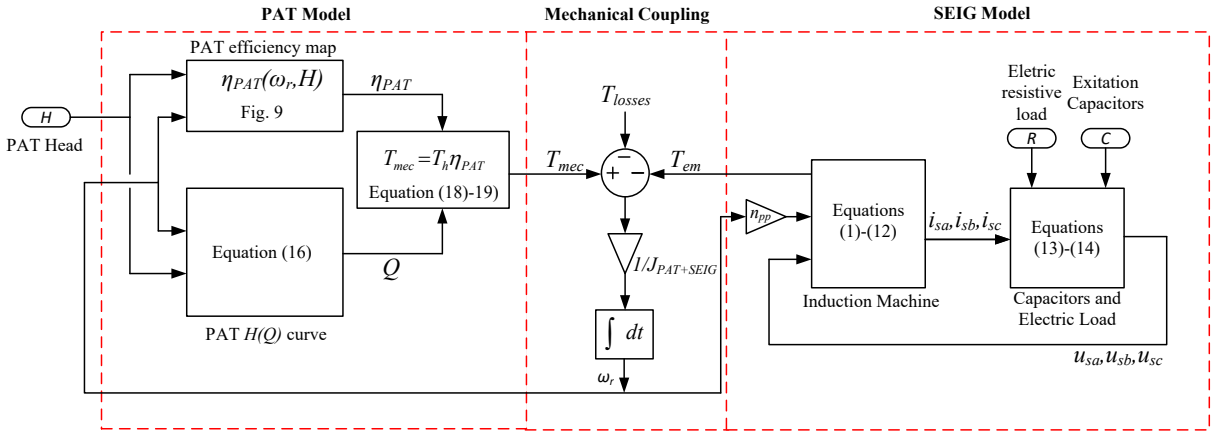

Fig. 7 – Schematic of the coupled PAT and SEIG dynamic models.

2.3 Series Connections of Pump as Turbine-Self-Excited Induction Generator Systems

As this work is multidisciplinary, combining two different scientific areas (PAT-hydraulic and SEIG-electric), it must be clarified that the series connection of PAT-SEIG system here analyzed is of the hydraulic type, as schematized in Fig. 8. Two sets of PAT-SEIGs are placed in series in the same hydraulic pipe, sharing the same flow rate, $Q_1 = Q_2 = Q$ and no significant pressure drop between them.

A series connection between two PATs has two principles that must be fulfilled. First, the flow leaving the outlet port of PAT1 has to be the same flow that enters the inlet port of PAT2: $Q_1 = Q_2$, where Q_1 is the flow rate from PAT1 and Q_2 is the flow rate in PAT2. Besides, the summation of the pressure drop associated with each of the two PATs has to be equal to the total pressure that is imposed on the system at any moment: $P_{total} = P_1 + P_2$, where P_1 corresponds to the pressure drop in PAT1 and P_2 to the pressure drop in PAT2. The model of the series connection between the two PATs must have this into account.

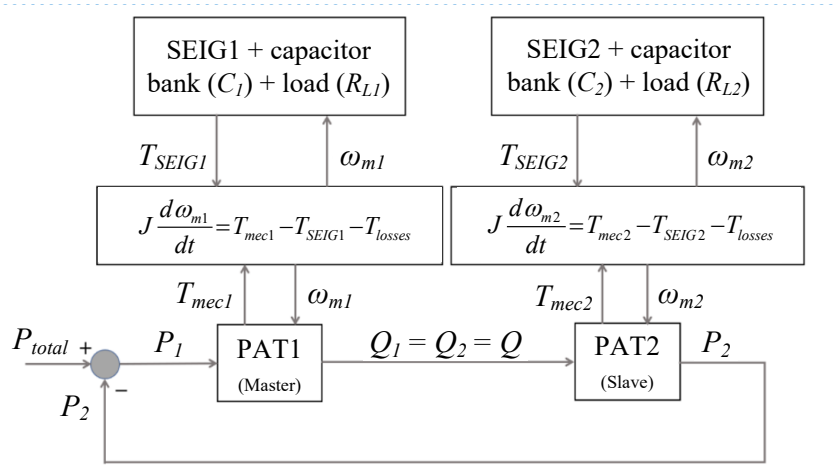

Fig. 8 – Model for the series connection between two PAT-SEIG systems: PAT1-SEIG1 and PAT2-SEIG2. Each subsystem comprises a PAT mechanically coupled to a SEIG, and the series connections are established between the two PATs. This series connection assumes no pressure drop between PAT1 and PAT2.

From a modeling point of view, each PAT would require its pressure to compute its flow rate. However, the pressure distribution between the two PATs is only determined after computing the rated flow and the electric operation point of each SEIG. Therefore, a master-slave methodology was used to solve this, where PAT1 is the master and PAT2 is the slave. The model for PAT1 is the same developed in section 2.2, where the input is the PAT1 pressure, P_1. However, the PAT2 model must be adapted to receive the flow rate Q_2 as input and not the pressure P_2. This can be easily done using (15) instead of (16) to compute the PAT2 pressure from its flow rate. This is illustrated in Fig. 8. At first glance, each SEIG (SEIG1 and SEIG2) seems independent. However, this is not true because, for example, if SEIG2 electrical load is increased, this will change the flow rate of PAT2, which, due to the hydraulic series connection, will influence the working point of PAT1-SEIG1.

A set of numerical studies were performed to understand this system's hydraulic-electric behavior (series connection). Each one starts by imposing a fixed pressure on the system. In the beginning, each generator was connected to a capacitor bank with equal capacitance C per phase and a resistive load R_L. As initially, C and R_L values are equal for both groups PAT+SEIG. The two PATs and SEIGs are equal (i.e., same hydraulic and electromechanics characteristic curves), the system always converged to the same operating point in each of the two groups. In this case of series connection specifically, the system evolved so that when the steady-state was reached, the system's pressure was equally divided between the two PATs. After the system stabilized, a perturbation was imposed to only one subsystem (PAT2 was used to include the perturbation). To be more specific, these perturbances were the variation in the capacitance value C_2 or a variation in the resistive load R_{L2}. The subsystem's choice in which the variation is applied is irrelevant, given that both subsystems are equal. The analysis of how the complete generating system reacts to the disturbance in the PAT-SEIG groups is described and discussed in the next section. Each plot and each notation that will be clarified next have to be considered, presuming the complete generating already reached an equilibrium initially when all the hydraulic and electrical components were the same. The variables resultant from the simulated tests are to be shown over time but only for a specific timespan, only during the transient when the parameters C or R_L were changed. The first part regarding the transient in which the SEIG excites and the two PATs converge to the same flow rate is not shown here.

3 Results and Discussion

This section presents the experimental validation of the SEIG and PAT models and the analysis of the results for the series connection between two PAT-SEIG groups when changing the operating point of one PAT-SEIG group. The objective is first to validate the PAT-SEIG models and then analyze the influence of a change of load or capacitor bank in the overall performance of the series-connected PAT-SEIG groups.

An error analysis was done using different error indexes. These are the Nash-Sutcliffe index (NSI), (20), and the Root Relative Squared Error (RRSE), (21). In these, E_i is the experimental value in each interval, $\bar{E}_i$ is the average of the observed values and S_i is the simulated value in each interval.

$$NSI = 1 - \frac{\sum_{i=1}^{N}[E_i - S_i]^2}{\sum_{i=1}^{N}[E_i - \bar{E}_i]^2} \tag{20}$$

$$RRSE = \sqrt{\frac{\sum_{i=1}^{N}[E_i - S_i]^2}{\sum_{i=1}^{N}[E_i - \bar{E}_i]^2}} \tag{21}$$

According to [32], it is possible to classify the results as "very good," "good," satisfactory," and "unsatisfactory" based on different ranges of the above indicators, Table 3.

Table 3 – Classification of best fit, according to [32]

Goodness Fit	NSI	RRSE
Very Good	NSI>0.6	0.00≤RRSE≤0.50
Good	0.40<NSI≤0.60	0.50< RRSE ≤0.60
Satisfactory	0.20<NSI≤0.40	0.60< RRSE ≤0.70
Unsatisfactory	NSI< 0.20	RRSE >0.70

3.1 Self-Excited Induction Generator Experimental Tests and Validation

Its electromechanical transient and steady-state responses were evaluated and compared with experimental results to validate the SEIG model. For this, a DC machine was chosen to be the prime mover, given its simple speed control. The simulation model of the SEIG coupled to the DC machine was developed, and the numerical results were compared with the experimental ones. The experimental setup developed in [23], Fig. 9, was used to measure the electromechanical dynamic behavior of the SEIG to validate the developed dynamic model.

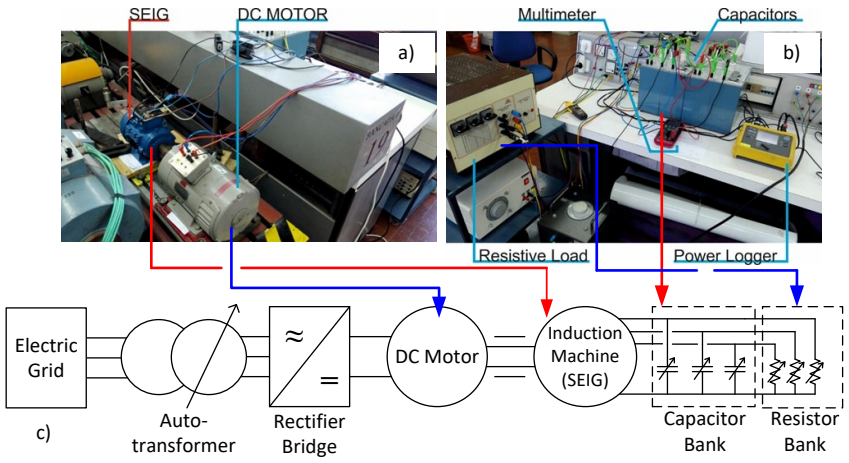

Fig. 9 – Experimental setup used to validate the SEIG numerical model: (a) the DC motor coupled to the SEIG, (b) the excitation capacitor bank and resistive load used for the SEIG, and (c) a schematic of the experimental setup.

Table 4 – Nameplate data of DC machine.

Rated Power	1.2 kW
Voltage	230 V
Current	5.2 A
Exc. Current	0.67 A
Rated Speed	1500 rpm

Two sets of experimental tests were carried to evaluate the SEIG model: 1) the first set consisted of the starting excitation of the SEIG, while 2) the second involved a transient response to a discontinuous change of resistive load. For the first experiment, the SEIG is started without the excitation capacitors and resistive load. The SEIG speed is increased until reaching its rated value by acting in the DC motor. After reaching the steady-state, the capacitors are connected, and the transient behavior of the stator voltage and current were registered. The same methodology was applied using the SEIG model. Fig. 10 shows the SEIG stator voltage (blue: experimental; red: simulation) when two different capacitor banks are connected. Fig. 6(a) was obtained with C = 50 μF and Fig. 6(b) with C = 80 μF. Both simulations follow the experimental results, presenting similar time constants and differences of 0.7 % and 4.4 % between the model's results and the measured experimental ones for the steady-state stator voltage amplitudes with different capacitors, respectively, C = 50 μF and for C = 80 μF. Using the NSI and RRSE indicators, results show very good results for both the values of the capacitors (NSI = 0.96 and RSEE = 0.21 for C = 50 μF and NSI = 0.93 and RSEE = 0.26 for C = 80 μF).

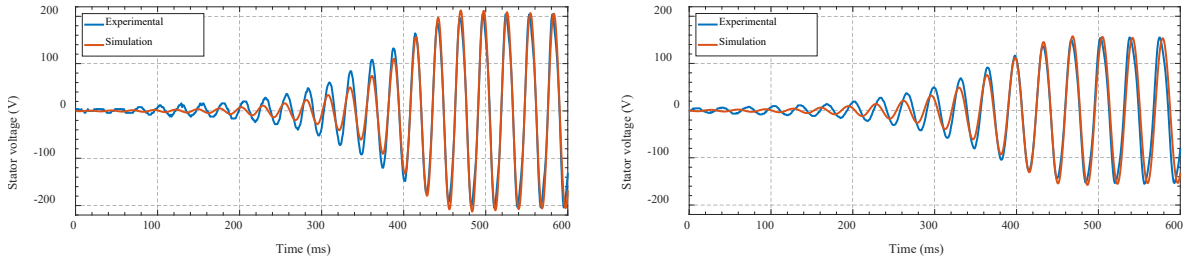

(a) (b)

Fig. 10 – SEIG stator voltage during the self-excitation process with: (a) C = 50 μF and (b) C = 80 μF. In blue, the experimental results. In red, the simulation ones.

After the self-excitation process and reaching its steady-state, a resistive load was applied to the SEIG, and its transient behavior was studied. In these tests, resistive loads of R_L = 600 Ω and R_L = 300 Ω are used. Fig. 11(a) and (b) present the experimental and simulation results after applying each resistive load. As it can be seen, the transient behavior is very similar in both experimental and simulation results, and the difference between steady-state stator voltage amplitudes is 0.6% for R_L = 600 Ω and 5.8 % for R_L = 300 Ω. The electric resistance R_L = 300 Ω is the one leading to the SEIG rated current. Further transient experimental tests were made [31]. Using the NSI and RRSE indicators, results show good results for both the values of the capacitors (NSI = 0.63 and RSEE = 0.60 for R_L = 600 Ω and NSI = 0.69 and RSEE = 0.39 for R_L = 300 Ω). These experimental results validated the developed SEIG model.

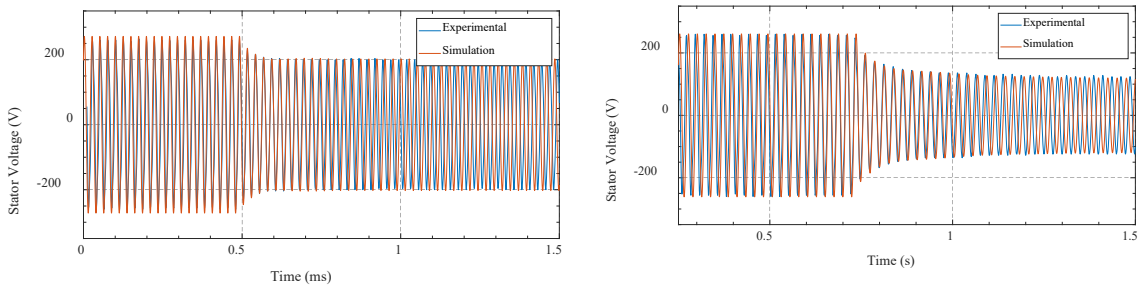

(a) (b)

Fig. 11 – SEIG stator voltage before and after applying a resistive load: (a) R_L= 600 Ω and (b) R_L=300Ω. In blue, the experimental results. In red, the simulation ones.

3.2 Pump as Turbine and Self-Excited Induction Generator Experimental Tests and Validation

To validate the PAT-SEIG system model, a set of experimental tests was carried out in the Laboratory of Hydraulic (IST, Portugal), using the experimental setup developed in [23] and [31]. During these tests, the PAT's stator voltage and electric frequency were acquired during transients and compared with the results from the simulation models.

First, a differential head of 5.82 m.w.c. was applied at PAT's terminals without the capacitor bank and an electric load connected at the SEIG terminals. After reaching the steady state, a capacitor bank of 17.5 μF was connected to the SEIG to start its self-excitation process, still without any electric load. The experimental and simulation transient behaviors of the SEIG stator voltage and its electric frequency during this operation are shown in Fig. 12(a)-(b). The build-up process of the stator voltage is seen, stabilizing at a voltage around 250 V, with similar behaviors for both experimental and simulation results. With the capacitor bank introduction, a reactive current is injected into the SEIG, increasing losses and reducing the electric frequency from 80 Hz to around 55 Hz, as shown in Fig. 12(b).

Another test was carried out, starting now with a capacitor bank of 34.7 μF and also a resistive electric load of $R_L = 300\ \Omega$ (rated-load), Fig. 12(c)-(d). With a resistive load, the transient regime during the SEIG excitation process is more oscillatory and requires more time to reach the steady-state, as shown in Fig. 12(c). Also, the steady-state regime is characterized by a lower stator voltage but with a similar electrical frequency, Fig. 12(d). In conclusion, the simulation model can provide accurate enough results for both extreme conditions: no-load load ($R_L = \infty$) and full load ($R_L = 300\ \Omega$). Additional tests were carried out in [31] to validate the developed model. According to the NSI and RRSE indicators, very good results were obtained for all quantities, Table 4.

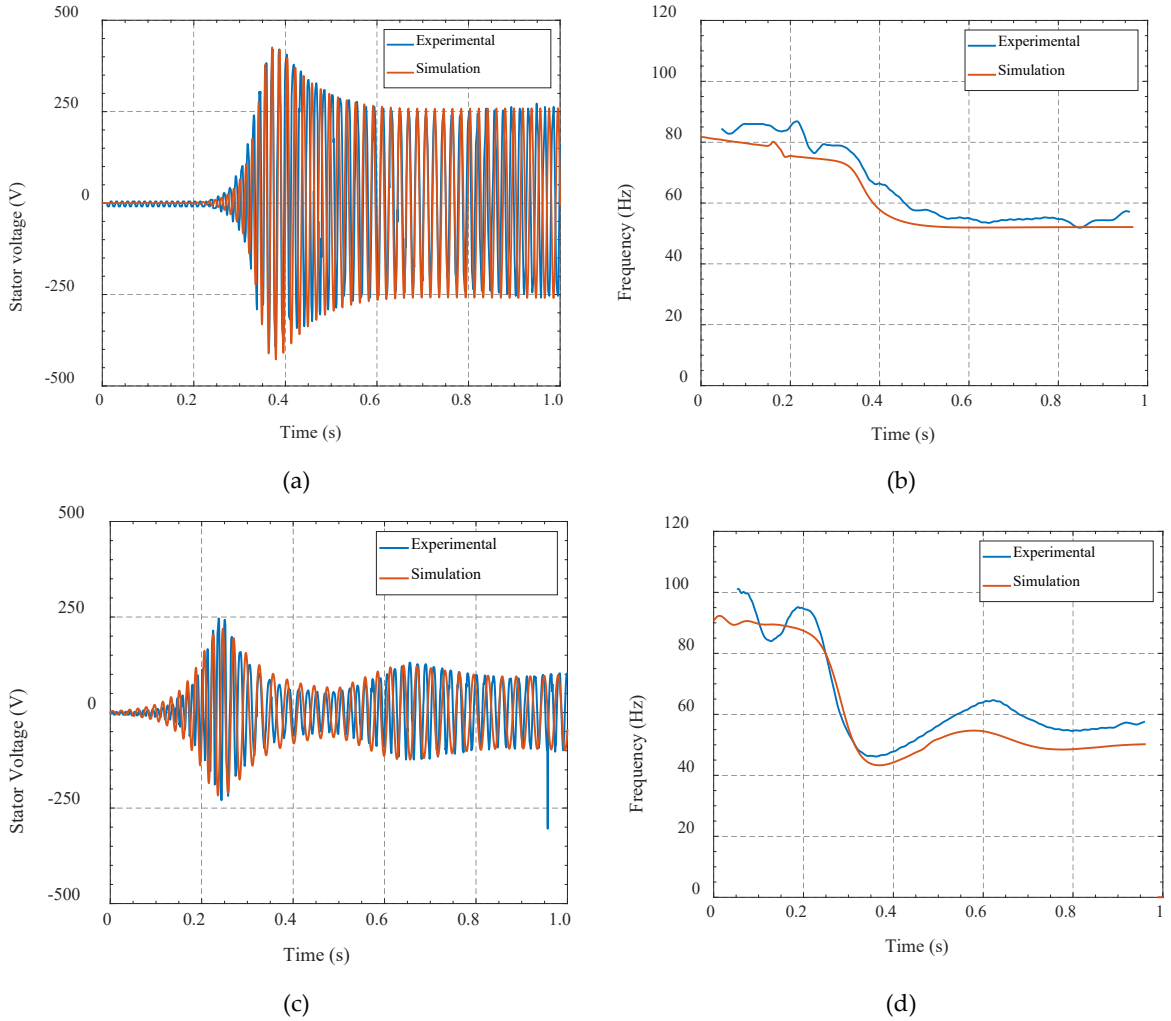

Fig. 12 – PAT-SEIG stator voltage during excitation with: (a) $C = 17.4$ μF, $R_L = \infty\ \Omega$ and and $H = 5.82$ m.w.c. and (b) $C = 34.7$ μF, $R_L = 300\ \Omega$ and $H = 7.5$ m.w.c. In blue, the experimental results. In red, the simulation ones.

Table 5 – Error analysis for PAT-SEIG experimental tests

Indexes	Stator voltage Fig. 12(a)	Frequency Fig. 12(b)	Stator voltage Fig. 12(c)	Frequency Fig. 12(d)
NSI	0.96	0.80	0.80	0.84
RRSE	0.20	0.45	0.44	0.40

3.3 Results Analysis for the Series Connection Between Groups

The analysis of the results for the series connection between the two PAT-SEIG groups is divided into two categories: 1) the effect of increasing C or R_L, and 2) the decrease of C or R_L. The results are grouped in this way since increasing C or R_L in one PAT-SEIG group has a similar effect on the other subsystem, and the same applies for decreasing C or R_L. Only one case from each result group (C – R_L) is presented in this current work. For simplicity, subscripts A and B will be adopted to refer to the operating point before (A) and after (B) the change in the PAT-SEIG system, respectively.

3.3.1 Decrease of Resistive Electric Load

To show the consequences of decreasing the value of one PAT-SEIG's electric load (R_L) on the power generating system, a specific test is studied. In this case, the pressure imposed to the series-connected system is $P_{total} = 5\times10^5$ Pa, the capacitance value $C_1 = C_2 = 23$ µF, and the electric load initially settled at $R_{L1} = R_{L2} = 200$ Ω. After the system reached its steady state, the load connected to SEIG2 was changed to $R_{L2} = 160$ Ω (simulating an increase of electric load). The rest of the parameters remained unchanged.

As explained in detail in [23], for each resistive load value, there is a capacitance-speed (C-N) relation that sets for each speed N the minimum C capable of guaranteeing the induction machine's self-excitation. Fig. 13(a) shows the (C-N) curves associated with each resistive load: (A) before ($R_{L2} = 200$ Ω) and (B) after changing the load ($R_{L2} = 160$ Ω). With a decrease of electric resistance connected to the SEIG, the (C-N) curve (A) is shifted to the right, as seen in Fig. 13(a), curve (B). Therefore, for a fixed value of the capacitor connected to SEIG2, C_2, a decrease in the R_{L2} will increase the induction generator speed from N_A to N_B. Fig. 13(b) shows the transient behavior of the SEIG2 rotor speed, N_2, after reducing the electric resistance value at $t = 2$s. Given this variation in the electrical load, the SEIG2 reacted by increasing the speed from $N_A = 1318$ rpm to $N_B = 1569$ rpm.

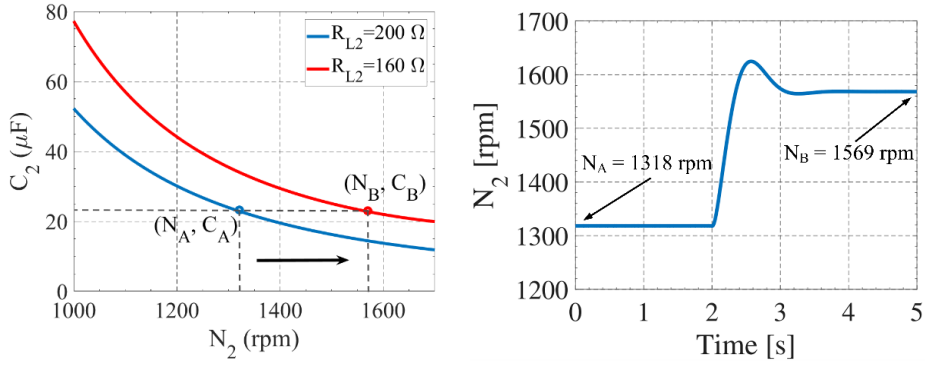

(a) (b)

Fig. 13 – (a) Generic representation of the curve's change relating to the minimum capacitance required to excite the SEIG2 with the mechanical speed N_2 when the value R_{L2} is decreased. (b) Evolution of the mechanical speed N_2 over time, during a decrease of 20% of R_{L2}.

As SEIG2 and PAT2 are mechanically coupled, there is a dependency between electrical and hydraulic systems. As shown previously, a change in the rotational speed causes a shift in the PAT's Q-H curve. More specifically, in this case for PAT2, as the speed increases, the curve corresponding to the operating point B will be above the operating point A, as shown in Fig. 14(a). As the two groups of PAT+SEIG are series-connected, the perturbation imposed on one group will also cause a change in the second group's operation. Due to this hydraulic series connection, the change in flow and head of PAT2 imposes a change in flow and head on PAT1, since it must be

guaranteed that the flow is the same ($Q_1 = Q_2$) for the two PATs and that the sum of the pressure drop remains unchanged ($P_{total} = P_1 + P_2$). For a similar reason, the changes verified in PAT1 also influence the operation of PAT2. Therefore, the two PATs interact with each other until the whole generating system converges to an equilibrium operating point. However, the speed of the two PAT-SEIG groups, N_1 and N_2, is not directly connected, i.e., they can have different speeds.

Fig. 14(a) shows that, as the resistance R_{L2} decreases, the speed N_2 increases. Considering the Q-H curves for PAT2, as N_2 increases, the flow Q_2 tends to decrease. Of course, this affects PAT1, given that $Q_1 = Q_2$. Therefore, looking at the Q-H curves for PAT1, in Fig. 14(b), it can be perceived that a drop in the flow rate Q_1 leads to a decrease of the head of PAT1, H_1. Promptly, this hydraulic adjustment in PAT1 will also have consequences in PAT2. As the head in PAT1 decreases, the head in PAT2, H_2, increases to maintain constant the total system pressure. At the same time that H_2 increases, the flow rate Q_2 continues to decrease, and this whole process repeats. This evolution of the coupling operation between the two PATs is distinguished in Fig. 14. Each PAT's progression is represented from point A to point B, including intermediate points (small red 'o' symbols).

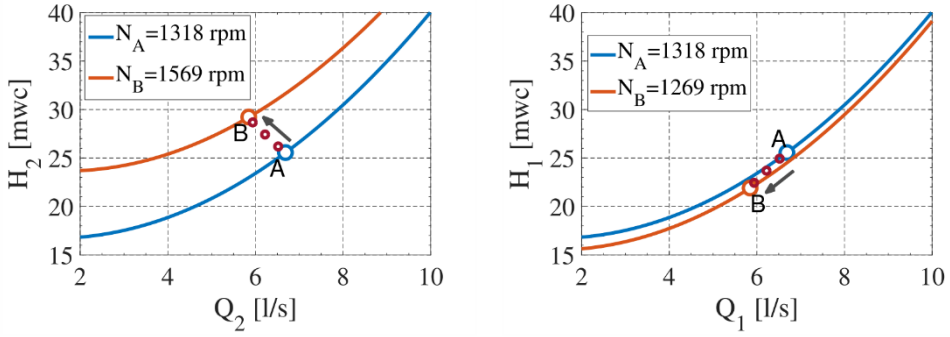

(a) (b)

Fig. 14 – Q-H characteristic curves of (a) PAT2 and (b) PAT1, before (A) and after (B) the decrease of R_{L2} , and intermediate points of the operation of each PAT (in red).

Fig. 15 shows how the head, flow, hydraulic and active power, and the system efficiency behave at each PAT-SEIG when going from (A) to (B). In PAT-SEIG2, where the variation of the load is applied, the flow decreases by 13 %, Fig. 15(a), and the head increases by 14 %, Fig. 15(b), resulting in the same hydraulic power after the change, Fig. 15(c). However, due to the series connection between groups, there is a significant variation of operation in the PAT-SEIG1. As both groups share the same flow, the flow in PAT-SEIG1 also decreased about 13 %, Fig. 15(a), but the head on this group increased 14 %, Fig. 15(a), to compensate for the decrease of PAT-SEIG2's head. The total head of the series-connected group should remain the same. Consequently, the hydraulic power transferred to PAT1, $P_{hyd1} = \rho g Q_1 H_1$, decreased by 25 %, and the one transferred to PAT2, $P_{hyd2} = \rho g Q_2 H_2$, converged to its initial value, Fig. 15(c). This means that decreasing the electric resistance of PAT2 does not significantly change its hydraulic power, P_{hyd2}, but the hydraulic power transferred to PAT1 decreases, P_{hyd1}.

Consequently, SEIG1 supplies the load R_{L1} with a much lower active power than the power delivered by SEIG2 to the load R_{L2}. Before the perturbation, each SEIG was supplying the load with P_s = 852W. When R_{L2} decreased by 20%, the active power that SEIG2 delivered to R_{L2} slightly decreased to P_{s2} = 790W (−7.3%), while the active power that SEIG1 delivered to R_{L1} already decreased to P_{s1} = 631W (−25.9%). Furthermore, the PAT-SEIG2 group's efficiency converged to its initial value after a transient, and the PAT+SEIG1 efficiency decreased from 51.1% to 47.1% (−7.8%). This brings an interesting conclusion: even though the load was changed in the second group PAT2+SEIG2, the highest impact is seen in the first group PAT1+SEIG1.

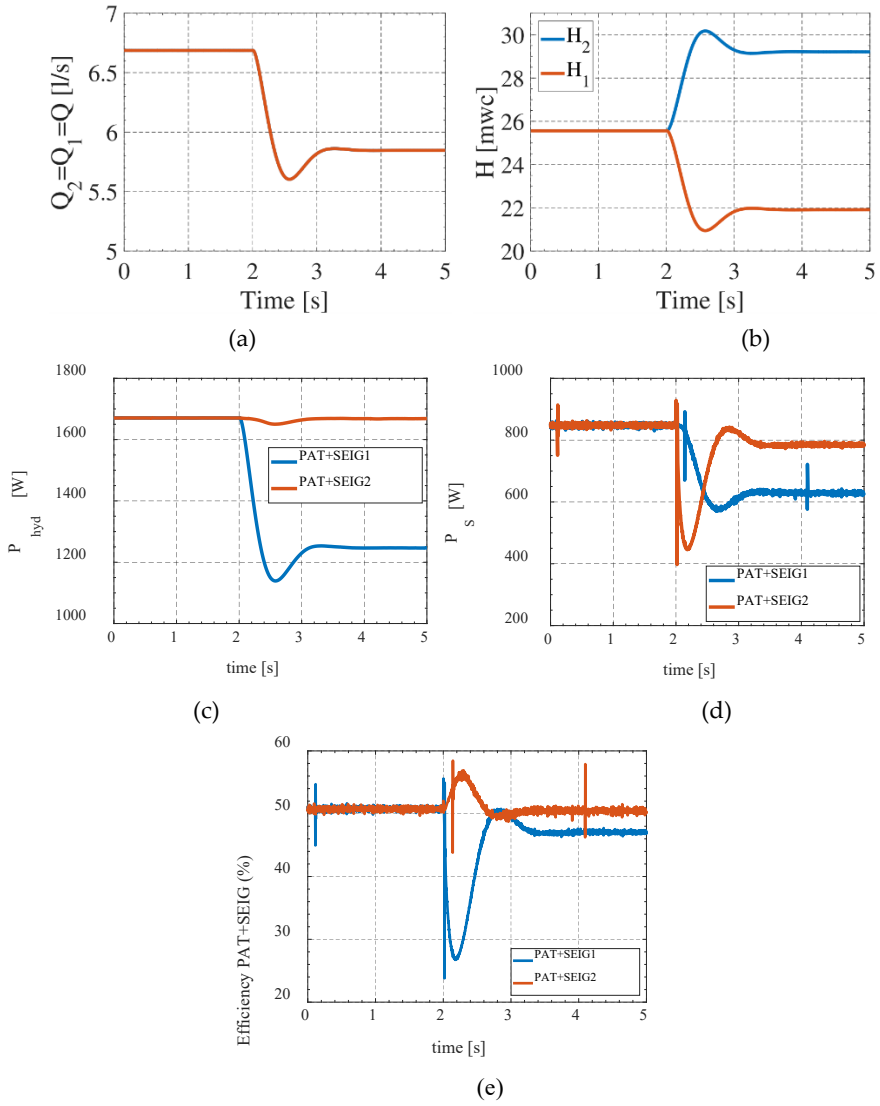

Fig. 15 – Results for the (a) flow rate Q, (b) head H, (c) hydraulic power, (d) active power and (e) system efficiency obtained in the simulation, captured during the decrease of R_{L2} by 20%.

3.3.2 *Increase of Capacitance*

This test very much resembles the test described for the decrease in R_{L2}. That is, the same total pressure $P_{total} = 5\times10^5$ Pa was imposed on the system, and the same initial capacitance and resistances were selected: $C_1 = C_2 = 23$ µF and $R_{L1} = R_{L2} = 200$ Ω. As soon as the system achieved its steady-state condition, the capacitance value C_2 was increased by 20 %. As Fig. 16(a) shows, the system shifted from its current operating point (A), $N_A = 1318$ rpm, $C_A = C_2 = 23$ µF and $R_{L2} = 200$ Ω, to a new operating point (B), $N_B = 1215$ rpm, $C_B = 27.6$ µF (+20 %) and $R_{L2} = 200$ Ω. As the capacitance value, C_2, increased, the mechanical speed N_2 decreases, given that the load R_{L2} remained fixed. Fig. 16(b) shows the rotational speed reduction after increasing the capacitor value at $t = 2.5$ s.

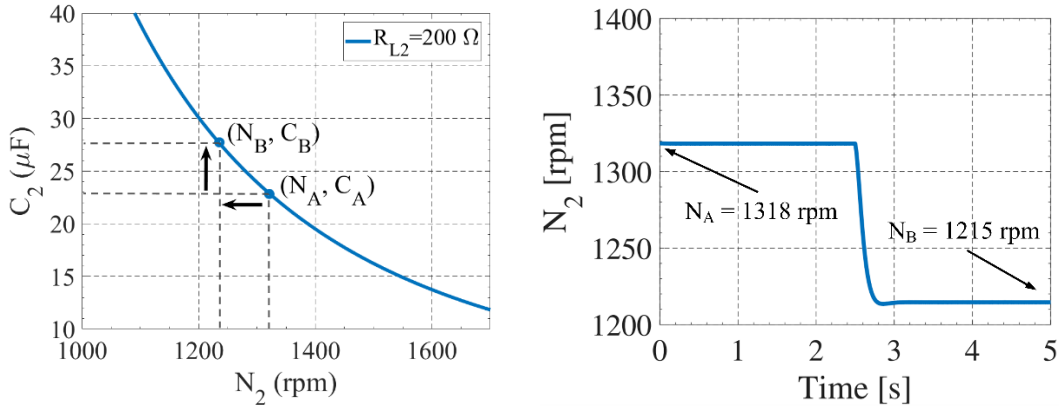

(a) (b)

Fig. 16 – (a) Generic representation of the change in the operating point of the SEIG2 when the capacitance C_2 is increased, seen on the curve relating the minimum capacitance required to excite the SEIG2 with the mechanical speed N_2, for a fixed load R_{L2}. (b) Evolution of the mechanical speed N_2 over time, during the capacitance C_2 by 20%.

As it was already perceived, when the two PATs are connected in series, this implies a dynamic dependency between them. When the two groups PAT+SEIG are connected to equal loads and capacitor banks, their outputs are the same. However, when a variation is imposed on one group, the other group will also be affected. It can be verified that, starting from the same conditions in the two groups, when the capacitance value C_2 is increased, the system evolved to decrease the mechanical speed N_2. Following this, the reaction of the second subsystem PAT1+SEIG1 to this variation in the group PAT2+SEIG2 is analyzed in detail.

Since PAT2 is mechanically coupled to SEIG2, the rotational speed of PAT2 decreased, and a shift in the *Q-H* curves occurs, Fig. 17(a). Here, as the speed decreased from N_A to N_B, the *Q-H* curve corresponding to the situation after the transient, N_B, is below the curve corresponding to the initial conditions, N_A. Observing each PAT's *Q-H* curves before and after the transient in Fig. 17, each one's evolution can be explained. Starting from point A, a decrease in the rotational speed causes an increase in the flow Q_2. As the two PATs are connected in series, they share the same flow rate. So, as Q_2 increases, does the flow in PAT1, Q_1. Following the *Q-H* curve's behavior in PAT1, as its flow Q_1 increases, so does the head H_1, as shown in Fig. 17(b). Since the sum of the heads in the two PATs must be constant for this specific connection, the increase in H_1 causes a decrease in the head of PAT2, H_2. With speed in PAT2 gradually decreasing, the flow rate Q_2 continues to increase, and this whole cycle repeats until the speed N_2 converges to N_B, which C_B dictates.

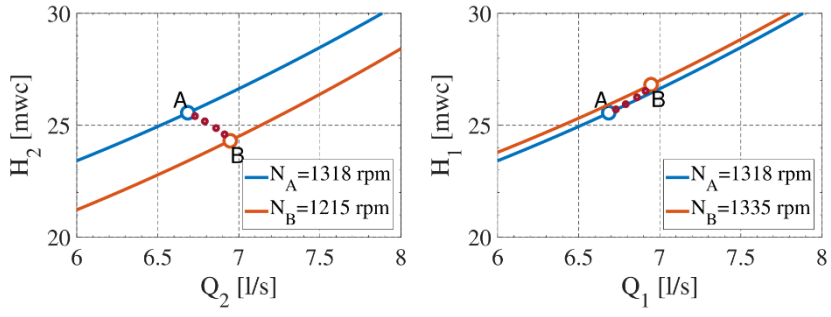

(a) (b)

Fig. 17 – Characteristic curves of (a) PAT2 and (b) PAT1, before (A) and after (B) the increase of C_2, and intermediate points of the operation of each PAT (in red).

The variation of the flow, head, hydraulic and active power and efficiency in each PAT-SEIG are shown over time in Fig. 18, with the variation of the capacitance C_2 at t = 2.5 s. Again, as the speed N_2 decreases, the PAT2 flow rate increases from 6.69 l/s to 6.95 l/s (+4 %). Accordingly, PAT1 reacted by increasing the head H_1 from 25.56 m.w.c. to 26.81 m.w.c. (+5 %). Given this, PAT1 forced the head H_2 to decrease by the same proportion (−5 %). Thus, the changes in flow and head for PAT2 cancel out again, leading to the same hydraulic power transferred to PAT2, P_{hyd2}, as before the perturbation occurs. Contrarily, as the changes in flow and head for PAT1

are both positive, this led to an increase in the hydraulic power of PAT1 of 9 %, Fig. 18(c). This increase in P_{hyd1} caused the rotational speed of PAT1, N_1, to increase over time.

Once again, it is proven in this test how the perturbation applied to the subsystem PAT2+SEIG2 has a higher influence in group PAT1+SEIG1 instead of its own. By increasing the capacitance value C_2 the PAT2 speed decreases and the active power P_{s2} transferred by SEIG2 to load R_{L2} slightly decreases from 852 W to 801 W (−6 %), Fig. 18(d). However, this change in C_2 caused an increase in the active power P_{s1} transferred by SEIG1 to its load R_{L1} from 852 W to 924 W (+8.4 %), but also slightly decreased the overall system efficiency, from 51.0 % to 48.6 %, Fig. 18(e).

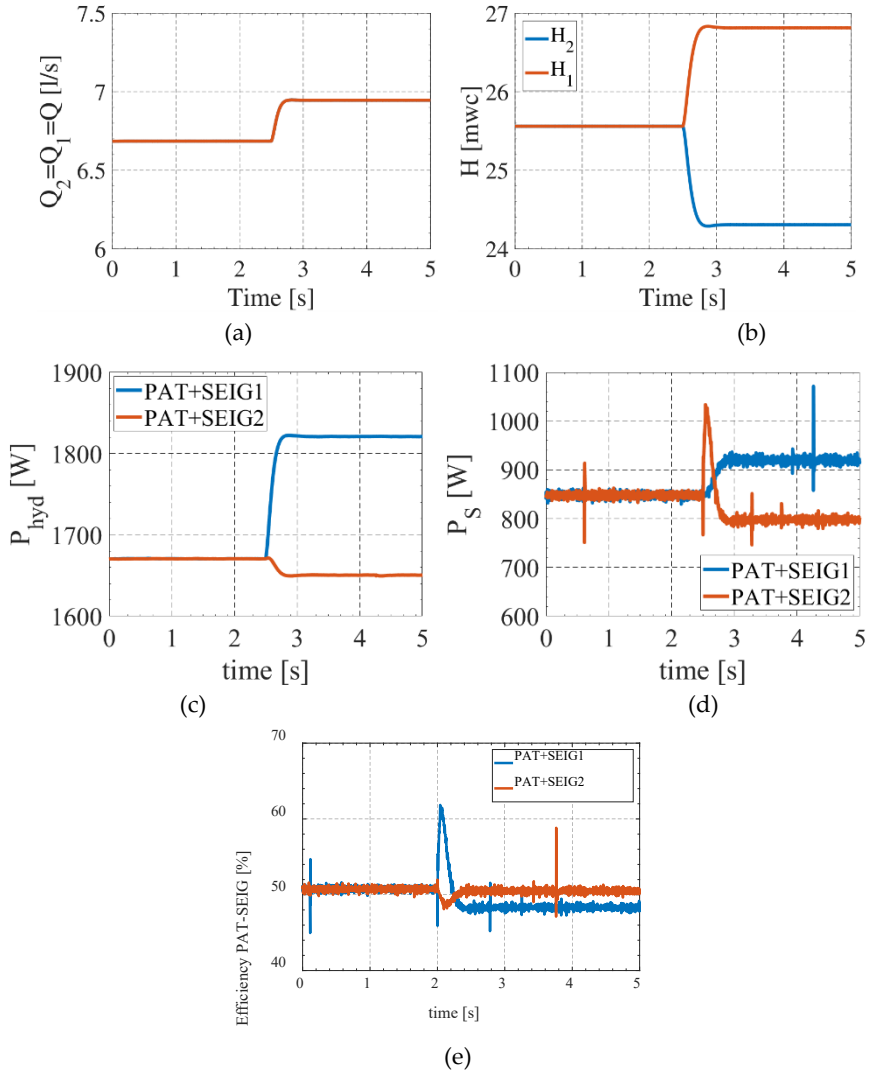

Fig. 18 – Results for the (a) flow rate Q, (b) head H, (c) hydraulic and (d) active power and (e) system efficiency, obtained in the simulation, captured during the increase of C_2 by 20%.

4 Discussion

This section presents the discussion of the results for the influence of the different variations of capacitors and resistive loads in a series connection between two PAT-SEIG systems. The results obtained for different variations of the capacitance C_2 are gathered in Fig. 19 and Fig. 20. These figures show how the hydraulic and active power, P_{hyd1}, P_{hyd2}, P_{s1} and P_{s2}, changes according to the variation of C_2. From it, it can be seen that as the variation of C_2

increased, both negatively and positively, the amplitude of the variation of P_{hyd1} and P_{s1} are most often higher than the amplitude of the variation of P_{hyd2} and P_{s2}, even though the perturbation was imposed to the group PAT2+SEIG2. Besides, these deviations in power were shown to be asymmetrical.

As for the results from the variation of R_{L2}, they were also gathered in Fig. 21 and Fig. 22. At the first sight, when comparing these figures with the previous ones, it can be noticed how these deviations of power have a lower amplitude. Moreover, the hydraulic and active power P_{hyd2} and P_{s2} remained constant to these variations in the load, even though the operating point changed. Also, these deviations were shown to be always negative. Regarding the subsystem where the perturbation was not imposed, PAT1+SEIG1 presents the same tendency as when the perturbation is the variation of the capacitance C_2. As demonstrated already, an increase in R_{L2} or C_2 led to increased hydraulic and active power P_{hyd1} and P_{s1}.

On the other hand, when R_{L2} or C_2 was decreased, P_{hyd1} and P_{s1} decrease. Again, the deviation from their original values increased as the negative variation of R_{L2} increased. Besides this, it is also worth mentioning that results were only shown for a maximum decrease of 20%, given that both SEIGs lost excitation when trying to decrease more the value of R_{L2}.

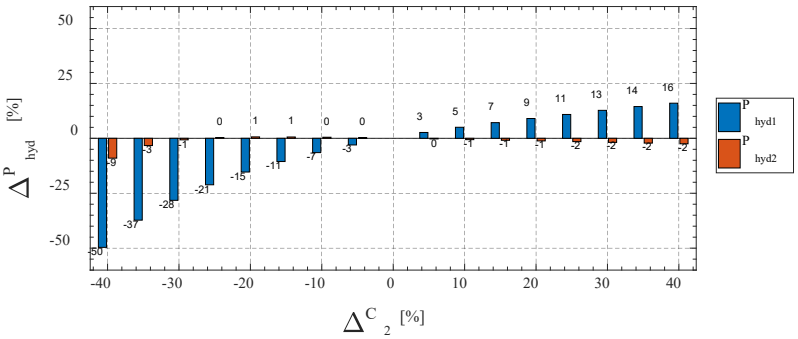

Fig. 19 – Consequences of the variation of the capacitance value C_2 on the hydraulic absorbed by both PATs.

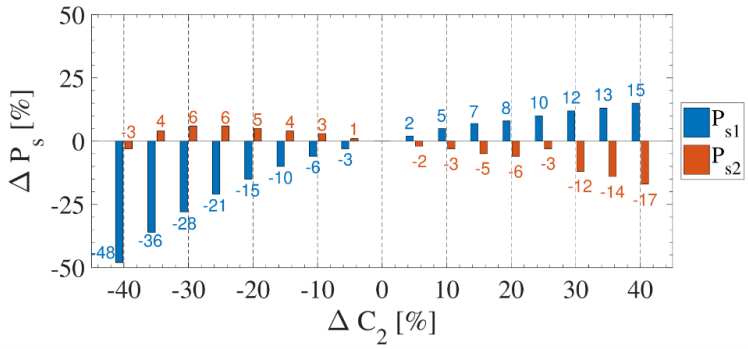

Fig. 20 – Consequences of the variation of the capacitance value C_2 on the active power delivered to the load R_{L1}, P_{s1}, and on the active power delivered to the load R_{L2}, P_{s2}.

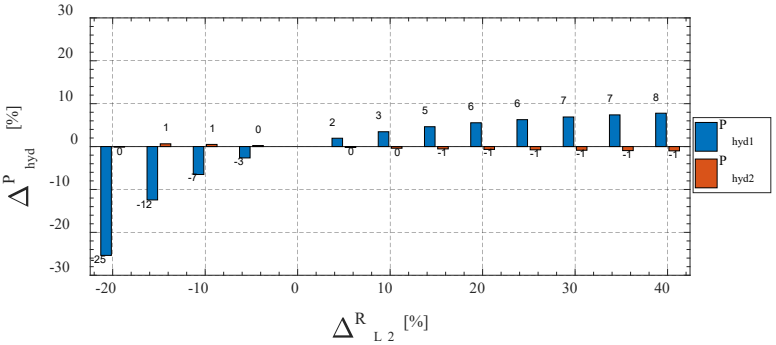

Fig. 21 – Consequences of the variation of the resistance value RL_2 on the hydraulic absorbed by both PATs.

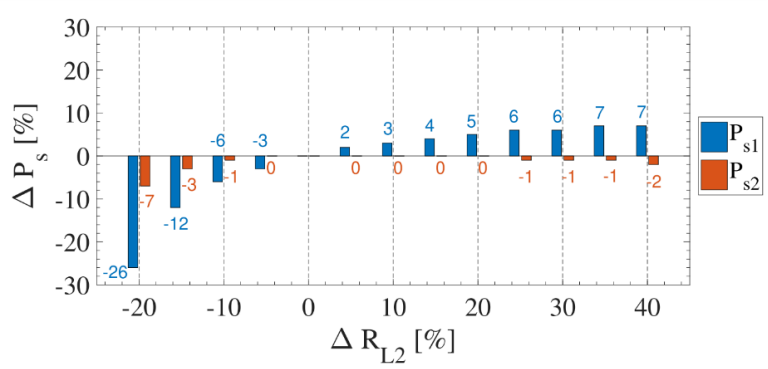

Fig. 22 – Consequences of the variation of the capacitance value R_{L2} on the active power delivered to the load R_{L1}, P_{s1}, and on the active power delivered to the load R_{L2}, P_{s2}.

From a reliability point of view, the control of off-grid PAT-SEIG systems with multiple groups in series is not straightforward. As one can change the value of the capacitor to regulate the hydraulic and active power of one independent PAT-SEIG, this cannot be said to be a group of series-connected PAT-SEIG systems. To regulate the hydraulic and active power of the PAT-SEIG2 group, one must act upon the capacitor (or resistance) of the PAT-SEIG1 group. Of course, this may not be feasible when these groups are far from each other in an off-grid system (example: different rural farms with the PAT-SEIG system installed). One possible solution is installing AC/DC inverters connected to batteries, with a control system capable of changing the reactive power injected to the SEIG to avoid external influences due to neighborhood PATs. This solution increases the cost of the PAT-SEIG system. It may not be economically viable for small applications, where the cost of the inverters and batteries would be higher than the PAT-SEIG system. When the PAT-SEIG groups are installed in the same facility, then, to regulate the hydraulic and active power of one PAT-SEIG, one must act upon the other PAT system, as shown in Fig. 19 to Fig. 22.

5 Conclusions

In this paper, a numerical model of an off-grid self-excited induction generator (SEIG) coupled to a pump working as a turbine (PAT) was presented and validated with success through a set of transient and steady-state experimental results. This modeling enabled a subsequent study of the series connection between two generating PAT-SEIG groups, from which the following conclusions can be drawn:

- For the particular PAT-SEIGs used, the series connection was demonstrated have relevant oscillating transients. In particular, the greater influence was verified in the adjacent PAT-SEIG group than in the group where the changes (resistive load or capacitances) were imposed.
- Changes led to different consequences depending if they were in the load or the bank of capacitors. A 40% increase in capacitances in one group leads to a 2% decrease in its hydraulic power. However, the hydraulic power in the other group increased by 16%. A 40% decrease leads to a decrease of 9% of the hydraulic power, instead of 2%, but a hydraulic power decrease of 50% in the other group. Similar behaviors were verified when the electric resistance load changed, however, with a lower impact.

From the anterior points, one concludes that the series connection of PAT-SEIGs is more vulnerable to changes in the excitation capacitance values than changes in the load. However, this conclusion can only be guaranteed to this specific generating system (of small power range). Nonetheless, to overcome this, future research is planned to conduct tests with the series connection in a high-power hydraulic system, where these mutual coupling effects maybe be mitigated.

Acknowledgments:

This work was supported by FCT, through IDMEC, under LAETA, project UID/EMS/50022/2020 and the project REDAWN (Reducing Energy Dependency in Atlantic Area Water Networks) EAPA_198/2016 from INTERREG ATLANTIC AREA PROGRAMME 2014-2020 and CERIS (CEHIDRO-IST), the Hydraulic Laboratory, for experiments on PATs. This research is also supported by the "Program to support the academic career of the faculty of the Universitat Politècnica de València 2019/2020 in the project 'A Step Ahead In Sustainability Of Water Systems For The Energy Transition In Communities` of the Modesto Pérez-Sánchez.

Conflicts of Interest:

The authors declare no conflict of interest.

The founding sponsors had no role in the design of the study, in the collection, analyses, or interpretation of data, in the writing of the manuscript, and in the decision to publish the results.

REFERENCES

[1] Krajačić, G., Vujanović, M., Duić, N., Kılkış, Ş., & Rosen, M. A. "Integrated approach for sustainable development of energy, water and environment systems". *Energy Conversion and Management*, 159, pp. 398-412, 2018.

[2] Capodaglio, A. G., & Olsson, G. "Energy issues in sustainable urban wastewater management: Use, demand reduction and recovery in the urban water cycle". *Sustainability*, 12(1), 266, 2020.

[3] Chen, S., & Chen, B. "Urban energy–water nexus: a network perspective". *Applied Energy*, 184, pp. 905-914, 2016.

[4] Wang, Y., Wang, J., Gao, M., Zhang, D., Liu, Y., Tan, Z., & Zhu, J. "Cost-based siting and sizing of energy stations and pipeline networks in integrated energy system". *Energy Conversion and Management*, 235, 113958, 2021.

[5] Gupta, A., Bokde, N., & Kulat, K. D. "Hybrid leakage management for water network using PSF algorithm and soft computing techniques". *Water resources management*, 32(3), pp. 1133-1151, 2018.

[6] Ramos, H., & Borga, A. "Pumps as turbines: an unconventional solution to energy production". *Urban Water*, 1(3), pp. 261-263, 1999.

[7] Novara D., McNabola A., "A model for the extrapolation of the characteristic curves of Pumps as Turbines from a datum Best Efficiency Point", *Energy Conversion and Management*, 174, pp. 1-7, 2018.

[8] Ramos, H., & Borga, A. "Pumps as turbines: an unconventional solution to energy production". *Urban Water*, vol. 1, no. 3, pp. 261-263, 1999.

[9] Rawal, S., & Kshirsagar, J. T. "Numerical simulation on a pump operating in a turbine mode". *In Proceedings of the 23rd international pump users symposium*, *Texas A&M University*. Turbomachinery Laboratories, 2007.

[10] Derakhshan, S., & Nourbakhsh, A. "Theoretical, numerical and experimental investigation of centrifugal pumps in reverse operation". *Experimental thermal and fluid science*, vol. 32, no. 8, pp. 1620-1627, 2008.

[11] Rossi, M., Nigro, A., & Renzi, M. "Experimental and numerical assessment of a methodology for performance prediction of Pumps-as-Turbines (PaTs) operating in off-design conditions", *Applied Energy*, vol. 248, pp. 555-566, 2019.

[12] Fecarotta, O., Ramos, H. M., Derakhshan, S., Del Giudice, G., & Carravetta, A. "Fine tuning a PAT hydropower plant in a water supply network to improve system effectiveness", *Journal of Water Resources Planning and Management*, vol. 144, no. 8, 04018038, 2018.

549 [13]Pokharel, N., Ghimire, A., Thapa, B. S., & Thapa, B. “Opportunity for research and manufacturing of pump
550 in Nepal”, *Journal of Physics: Conference Series,* 1608, no. 1, p. 012018, 2020.

551 [14]Pérez-Sánchez, M., Sánchez-Romero, F. J., López-Jiménez, P. A., & Ramos, H. M. “PATs selection towards
552 sustainability in irrigation networks: Simulated annealing as a water management tool”. *Renewable Energy*,
553 116, pp. 234-249, 2018.

554 [15]Shahin Ebrahimi, Alireza Riasi, Ali Kandi, “Selection optimization of variable speed pump as turbine (PAT)
555 for energy recovery and pressure management”, *Energy Conversion and Management*, 227, pp. 113586, 2021.

556 [16]Cimorelli, L., D'Aniello, A., Cozzolino, L., & Pianese, D. “Leakage reduction in WDNs through optimal
557 setting of PATs with a derivative-free optimizer”. *Journal of Hydroinformatics*, 22(4), pp. 713-724, 2020.

558 [17] Bekiloğlu, H. E., Bedir, H., & Anlaş, G. “Multi-objective optimization of ORC parameters and selection of
559 working fluid using preliminary radial inflow turbine design”. *Energy Conversion and Management*, 183, pp.
560 833-847, 2019.

561 [18] Samora, I., Franca, M. J., Schleiss, A. J., & Ramos, H. M. “Simulated annealing in optimization of energy
562 production in a water supply network”. *Water resources management*, 30(4), pp. 1533-1547, 2016.

563 [19] Chacón, M. C., Díaz, J. A. R., Morillo, J. G., & McNabola, A. “Estimating regional potential for micro-
564 hydropower energy recovery in irrigation networks on a large geographical scale”. *Renewable Energy*, 155,
565 pp. 396-406, 2020.

566 [20] Algieri, A., Zema, D. A., Nicotra, A., & Zimbone, S. M. “Potential energy exploitation in collective irrigation
567 systems using pumps as turbines: A case study in Calabria (Southern Italy)”. *Journal of Cleaner Production*,
568 257, 120538, 2020.

569 [21] Renzi, M., Rudolf, P., Štefan, D., Nigro, A., & Rossi, M. “Installation of an axial Pump-as-Turbine (PaT) in
570 a wastewater sewer of an oil refinery: A case study”. *Applied Energy*, 250, pp. 665-676, 2019.

571 [22] Williams, A.A. “Pumps as turbines for low cost micro hydro power”. *Renew. Energy*, 9, pp. 1227–1234, 1990.

572 [23] Capelo, B., Pérez-Sánchez, M., Fernandes, J. F., Ramos, H. M., López-Jiménez, P. A., & Branco, P. C.
573 “Electrical behaviour of the pump working as turbine in off grid operation”. *Applied Energy*, 208, pp. 302-311,
574 2017.

575 [24] Yaramasu, V., Dekka, A., & Rodriguez, J. “Modulated Model Predictive Torque and Current Control of
576 Squirrel Cage Induction Generator-Based Wind Power Generation System”. In *2020 IEEE 21st Workshop on*
577 *Control and Modeling for Power Electronics (COMPEL)* pp. 1-7, 2020.

578 [25] Fernandes, João F.P. ; Pérez-Sánchez, Modesto; Ferreira, F.; Ramos, Helena M.; López Jiménez, Petra
579 Amparo; Costa Branco, P.J. “Optimal energy efficiency of isolated PAT systems by SEIG excitation tuning”.
580 *Energy Conversion and Management*, 183, pp. 391 – 405, 2019.

581 [26] Hao Zhang, Pengcheng Guo, Longgang Sun, “Transient analysis of a multi-unit pumped storage system
582 during load rejection process”, *Renewable Energy*, Volume 152, pp. 34-43, 2020.

583 [27] Hao Zhang, Diyi Chen, Changzhi Wu, Xiangyu Wang, Jae-Myung Lee, Kwang-Hyo Jung, “Dynamic
584 modeling and dynamical analysis of pump-turbines in S-shaped regions during runaway operation”, *Energy*
585 *Conversion and Management*, vol. 138, pp. 375-382, 2017.

586 [28] Hao Zhang, Diyi Chen, Beibei Xu, Edoardo Patelli, Silvia Tolo, “Dynamic analysis of a pumped-storage
587 hydropower plant with random power load”, *Mechanical Systems and Signal Processing*, vol. 100, pp. 524-
588 533, 2018.

589 [29] Delgado, J., Andolfatto, L., Covas, D. I. C., & Avellan, F. “Hill chart modelling using the Hermite polynomial
590 chaos expansion for the performance prediction of pumps running as turbines”. *Energy Conversion and*
591 *Management*, 187, pp. 578-592, 2019.

592 [30] Kramer, M., Terheiden, K., & Wieprecht, S. “Pumps as turbines for efficient energy recovery in water supply
593 networks”. *Renewable energy*, 122, pp. 17-25, 2018.

[31] Madeira, F.C.; Fernandes, J.F.P.; Pérez-Sánchez, M.; López-Jiménez, P.A.; Ramos, H.M.; Costa Branco, P.J. "Electro-Hydraulic Transient Regimes in Isolated Pumps Working as Turbines with Self-Excited Induction Generators." *Energies*, 13, pp. 4521, 2020.

[32] Moriasi, B.; Arnold, J.; van Liew, M.; Binger, R.; Harmel, R.; Veith, T. "Model evaluation guidelines for systematic quantification of accuracy in watershed simulations". *Trans. ASABE*, vol. 50, pp. 885–900, 2007.